Ann. Geophys., 30, 911–926, 2012
www.ann-geophys.net/30/911/2012/
doi:10.5194/angeo-30-911-2012

Annales Geophysicae

Behavior of substorm auroral arcs and Pi2 waves: implication for the kinetic ballooning instability

T. F. Chang[1,2], **C. Z. Cheng**[1,3], **C. Y. Chiang**[2], **and A. B. Chen**[1,3]

[1]Plasma and Space Science Center, National Cheng Kung University, Taiwan
[2]Department of Physics, National Cheng Kung University, Taiwan
[3]Institute of Space, Astrophysical and Plasma Sciences, National Cheng Kung University, Taiwan

Correspondence to: T. F. Chang (jocelyn@pssc.ncku.edu.tw)

Received: 23 December 2011 – Revised: 11 May 2012 – Accepted: 14 May 2012 – Published: 4 June 2012

Abstract. We present synoptic observations of the 21 December 2006 substorm event by the THEMIS ground-based All-Sky-Imagers, the ISUAL CCD Imager aboard the FORMOSAT-2 satellite, the geosynchronous satellites and the ground-based magnetometers, and discuss the implication of the observations. There are three subsequent arc breakups with time separation of <1 min during the substorm expansion phase. In particular, we investigated the mode number of the substorm arc bead-like structure and the concurrent behavior of the arc intensity, the westward electrojet intensity, and the ground Pi2 pulsation amplitude. Prior to each arc breakup there was a clear azimuthally-spaced bright spot structure along the arc with high mode number (∼140–180) and the arc intensity increased together with the westward electrojet and the ground Pi2 pulsation amplitude under the arc. The Pi1 perturbations observed under the arc appeared at or after the arc breakup started. This suggests that the Pi2 pulsation is related to the arc formation. The Pi2 pulsation may be caused by the kinetic ballooning instability (KBI) that is excited in the strong cross-tail current region. The longitudinal extent of the earthward expansion front of the substorm dipolarization region at the geosynchronous orbit is estimated from timings of the energetic proton and electron injections and is roughly located between ∼19.50 MLT and ∼23.00 MLT, which is consistent with the corresponding longitudinal extent of the auroral substorm activity.

Keywords. Magnetospheric physics (Auroral phenomena; Storms and substorms)

1 Introduction

Decades of research have demonstrated that the substorm is a significant dynamical process of energy storage and release in the magnetosphere and ionosphere. However, the mechanism of substorm onset, which is most critical for understanding the dynamics of the plasma sheet and corresponding auroral activities from the growth phase to the expansion phase, still remained controversial.

The debate often raged over where, when, and how the substorm occurs in the magnetosphere. Observations and theories have so far led to two main morphological substorm models to describe the substorm onset and expansion processes: the near-Earth onset model (e.g., Lui et al., 1992; Lui, 1996) and the near-Earth neutral line (NENL) model (e.g., Baker et al., 1996). The NENL model asserts that the magnetic reconnection initiated outside 15 R_E in the magnetotail produces fast bursty bulk plasma flows which arrive at the near-Earth region with flow braking to cause substorm onset (e.g., Angelopoulos et al., 1992; Shiokawa et al., 1998). The near-Earth onset model proposes that some instabilities are initiated in the near-Earth plasma sheet to cause substorm onset and subsequent expansion (e.g., Lui et al., 1991; Roux et al., 1991; Samson et al., 1992; Cheng and Lui, 1998; Lee et al., 1998; Cheng and Zaharia, 2004; Cheng, 2004; Dobias et al., 2004; Lui, 2004; Saito et al., 2008). In particular, the theoretical calculation of ballooning instability in the 3-D magnetospheric equilibrium that models the growth phase magnetosphere showed that the low-frequency instability in the Pi2 frequency range has the maximum growth rate in the strong cross-tail current region, and the most unstable ballooning mode field line region can be traced to the ionosphere

in the transition region between the Region 1 and Region 2 currents (Cheng and Zaharia, 2004; Cheng, 2004).

The auroral arc formation and breakup are the manifestation of magnetospheric dynamics in the ionosphere, and are considered the most reliable substorm indicator (Liou et al., 1999, 2000; Lyons et al., 2002; Meng and Liou, 2004; Akasofu et al., 2010). Thus, detailed observations of the substorm auroral arc formation and breakup are essential to provide understanding of the physical mechanism of substorm onset. The POLAR Ultraviolet Imager (UVI) and the IMAGE Far Ultraviolet (FUV) Imager have provided global auroral images over the whole polar region, but typically with 1 min or longer time resolution and spatial resolution of 40 km for UVI and 60 km for FUV at apogee. Because the growth of substorm arcs typically lasts ∼1–3 min or shorter prior to breakup and the arcs have bright spot structure of <10 km, auroral observations with high temporal and spatial resolution are important to explore the structure and dynamical evolution of the substorm arc formation and breakup. Moreover, high resolution ground magnetic field observation under the auroral arc should provide additional information on the nature of the substorm auroral arc.

In this paper we present detailed observational features of an auroral substorm event that occurred over Alaska and western Canada on 21 December 2006. The auroral substorm evolution and its magnetic field features were observed by the THEMIS Ground Based Observatory (GBO) with unprecedented spatial resolution of ∼1 km at magnetic zenith and temporal resolution of 3 s cadence All-Sky-Imager (ASI) images and 2 samples per second ground magnetometer data (e.g., Angelopoulos, 2008; Mende et al., 2007, 2008), and by the CCD Imager of ISUAL (Imager of Sprites and Upper Atmospheric Lightnings) (e.g., Chern et al., 2003) aboard the FORMOSAT-2 satellite, which provided optical observation of the substorm, arc vertical structure from the side with a high cadence of 1.4 s with 1 s exposure and a high spatial resolution of ∼2 km pixel^{-1}. It is to be emphasized that ISUAL is the first space-based imager that observes vertical images of auroral activities with such high resolutions.

In the 21 December 2006 substorm event there were three subsequent arc growth and breakups before the full auroral expansion. Each arc growth lasted ∼1 min or shorter. When the arc appeared, the ground Pi2 pulsation (40–150 s period) was also observed under the arc simultaneously. Prior to each arc breakup, the arc showed azimuthally-spaced bright spots along the arc (Voronkov et al., 1999; Donovan et al., 2008; Liang et al., 2007, 2008; Uritsky et al., 2009; Sakaguchi et al., 2009; Henderson, 2009; Rae et al., 2009a, b, 2010) and the arc intensity increases with the Pi2 amplitude for several tens of seconds. The relationship between auroral onset and Pi2 pulsation was also studied by Kepko and McPherron (2001) and Rae et al. (2009a, b, 2010). The advantage of the present work is that we make use of simultaneous auroral observations by the ground-based THEMIS ASIs with the broad-band filter and the space-based ISUAL CCD Imager with the 630.0 nm filter. Both the ground-based and space-based observations show comparable spatial and temporal resolutions of the substorm arc. In particular, the exponential growth rate of the substorm arc intensity was similar in both the broad-band auroral observation (in GAKO observations) and the ISUAL 630.0 nm auroral observation during the arc intensification prior to the arc breakup. We have also investigated the mode number of the bead-like structure of the substorm arc and the concurrent increase of the arc intensity, the westward electrojet intensity, and the ground Pi2 pulsation amplitude.

The temporal correlation between the arc intensity and the Pi2 amplitude suggests that the Pi2 pulsation is related to the substorm auroral arc formation. Pi1 (1–40 s period) pulsations were observed several tens of seconds after the arc breakup started, indicating that the Pi1 pulsations are not the cause of arc formation and growth, but rather are the consequence of the arc intensification and breakup. Because in satellite observations Pi2 pulsations are usually observed prior to onset of substorm dipolarization in the plasma sheet and Pi1 pulsations are observed at or after the substorm onset (e.g., Takahashi et al., 1987; Roux et al., 1991; Cheng and Lui, 1998; Shiokawa et al., 2005), the Pi1 and Pi2 waves observed by satellites in the near-Earth plasma sheet and by ground-based magnetometers located under the arc may be the same phenomena. Because arc emission structures with high azimuthal mode number were observed along the intensifying arc, the instability (in Pi2 frequency range) responsible for producing the substorm arc must also have high azimuthal mode number. The westward electrojet is produced concurrently with the auroral arc and is confined inside the auroral arc, which supports the theory of the Cowling channel effect (e.g., Boström, 1964; Fujii et al., 2011; Yoshikawa et al., 2011) in the production of westward electrojet. From the energetic particle injection observed by the geosynchronous satellites, the azimuthal extent of the dipolarization region is consistent with the region of substorm auroral activity, which suggests that the auroral substorm region maps along field lines to the dipolarization region in the magnetosphere.

In the following we first describe the auroral substorm arc formation, growth and breakup. Then, we describe the ground magnetic field features under the substorm auroral arcs. Then, we describe the dispersionless energetic particle injection observed by geosynchronous satellites. Finally, a summary and discussion is given, and the kinetic ballooning instability is considered as the key mechanism that causes the substorm auroral arc formation, growth and breakup.

2 Observation overview

The 21 December 2006 substorm event started at ∼08:27 UT. Before the substorm, the solar wind had a steady speed ∼700 km s^{-1}, a dynamic pressure ∼1.88 nPa, and a

Table 1. Locations of the THEMIS All-Sky-Imager sites used for the 21 December 2006 substorm event study.

Site	Abbrev.	MLAT	MLT
Kiana	KIAN	65.08°	20.93
Gakona	GAKO	63.38°	21.97
White Horse	WHIT	64.01°	22.61

southward interplanetary magnetic field ∼2 nT. The Dst and Kp indices were −28 nT and 3+ at 08:00 UT, respectively. The AU and AL indices with 1 min resolution during this interval are shown in Fig. 1a. The AL index started to decrease significantly from ∼ −400 nT at ∼08:28 UT, indicating a noticeable growth of westward electrojet associated with the substorm (Wien and Gordon, 1975). The substorm aurora appeared at ∼21.00 MLT and ∼65.5° MLAT and lasted for ∼30 min. The AL index reached its lowest value of ∼ −970 nT at ∼08:34 UT and then returned to the quiet time level of ∼ −100 nT at ∼08:55 UT.

The substorm auroral activities were over Alaska and western Canada. The auroral substorm was observed by three ground-based THEMIS ASIs located at Kiana (KIAN), Gakona (GAKO), and White Horse (WHIT) and their locations are listed in Table 1. The auroral substorm was also observed from the sideway by the ISUAL CCD Imager aboard the FORMOSAT-2 satellite in a sun-synchronized orbit at ∼890 km altitude with 99° inclination angle. When the FORMOSAT-2 satellite moved from south to north at ∼20:00 MLT, the track of ISUAL field-of-view (FOV) projection overlapped with part of the FOVs of THEMIS ASIs at GAKO and WHIT. There was an evident negative H-bay observed by the ground-based magnetometers, located roughly along the Alaska-Canada border region. Dispersionless energetic particle injections associated with the substorm were also observed by the geosynchronous satellites 1989-046, 1994-084 and LANL-97A with 60 s temporal resolution. To estimate these geosynchronous satellite locations relative to the substorm dipolarization region, their field line footprints are mapped to the ionosphere based on the T96 magnetic field model at ∼08:28 UT and are marked as solid triangles in Fig. 1b. The field line footprint of the LANL-97A geosynchronous satellite was located in the early evening sector (∼19:00 MLT) and the field line footprints of the 1989-046 and 1994-084 geosynchronous satellites were located in the pre-midnight sector (∼23:00 MLT). Figure 1b shows the locations of the ground-based magnetometers (solid dots), the field line footprints of the FORMOSAT-2 satellite (empty squares) and the ISUAL FOVs (trapezoids), and the FOVs of the THEMIS ASIs (circles). The auroral substorm activity was located in the local time sector from 19:00 to 23:00 MLT.

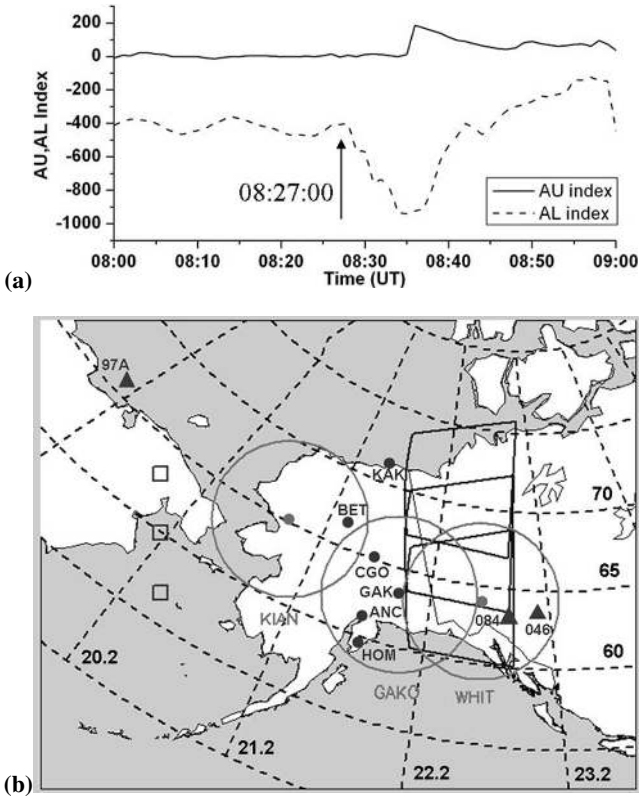

Fig. 1. (a) AU and AL indices during the 21 December 2006 substorm; **(b)** Locations of the ground-based All-Sky Imagers (ASIs, shown as grey solid circles) at KIAN, GAKO and WHIT, magnetometer sites (shown as dark solid circles) at Kaktovik (KAK), Bettles (BET) and College International Geophysical Observatory (CGO), Gakona (GAK), Anchorage (ANC), and Homer (HOM), and field line footpoints of geosynchronous satellites (LANL-97A, 1994-084, 1989-046 shown as solid triangles) and FORMOSAT-2 satellite (shown as squares). Large circles are the FOVs of the ASIs. The FOVs of ISUAL aboard the FORMOSAT-2 are shown as trapezoids.

3 Observation by THEMIS All-Sky-Imagers

Figure 2a and b shows the auroral substorm activity observed by the ground-based THEMIS ASIs located at KIAN, GAKO, and WHIT. The entire sequence of images is given in supplementary material Animation S1. Before the auroral substorm started at ∼08:27:09 UT, there was a pre-existing arc located at ∼66° MLAT which remained undisturbed and extended azimuthally in the FOVs of these three ASIs. At ∼08:26:36 UT, there was an east–west localized faint aurora spot located on the equatorward side of the pre-existing arc in the KIAN FOV. The faint aurora propagated westward to the edge of KIAN FOV, but its location is still on the poleward side of the substorm initial initiation arc. Then, the substorm initiation arc was observed at ∼08:27:09 UT with several identifiable brightening spots along the brightening arc on the equatorward side (at

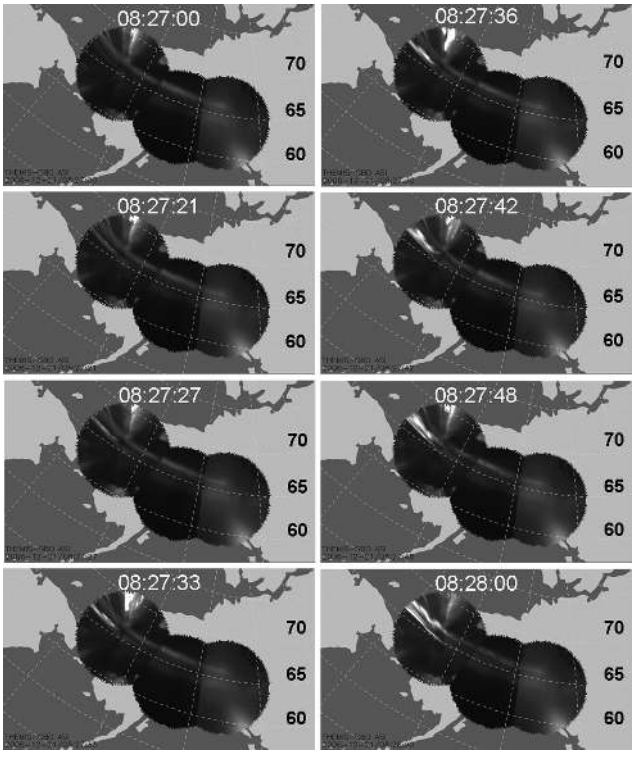

Fig. 2a. Evolution during 08:27:00–08:28:00 UT of the 21 December 2006 auroral substorm event observed by the THEMIS ground-based All-Sky-Imagers located at KIAN, GAKO, and WHIT.

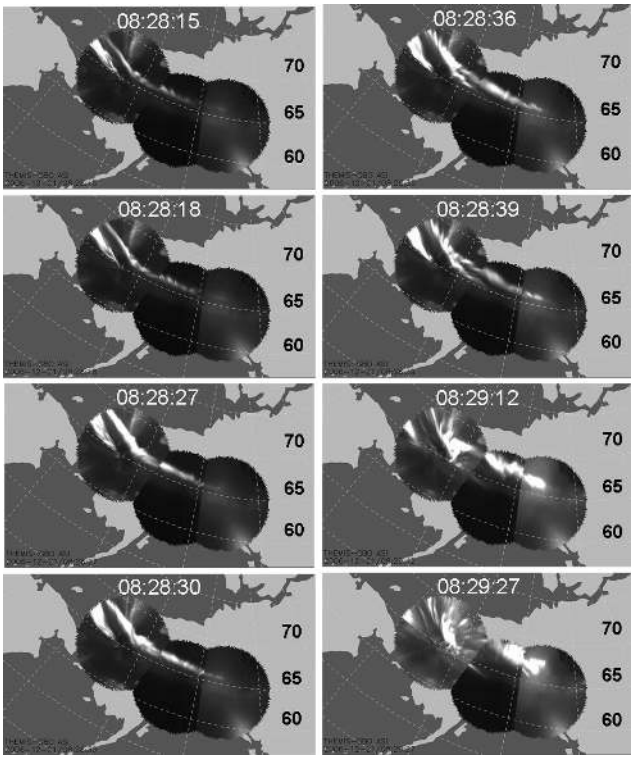

Fig. 2b. Evolution during 08:28:15–08:29:27 UT of the 21 December 2006 auroral substorm event observed by the THEMIS ASIs located at KIAN, GAKO, and WHIT.

∼65.5° MLAT) of the pre-existing arc in the western part of KIAN FOV. The arc intensified exponentially and then broke up into two arcs at ∼08:27:48 UT. The lower breakup arc remains at the original arc latitude, but the upper breakup arc quickly moved poleward to the pre-existing arc latitude at ∼08:28:00 UT. Then, the poleward-side breakup arc quickly brightened and extended eastward into the GAKO ASI FOV and then to the WHIT ASI FOV. As the breakup arc extended eastward, its intensity also increased exponentially with bead-like structure brightening spots along the brightening arc during 08:28:09–08:28:33 UT, and these brightening spots were approximately equally spaced along the arc. At ∼08:28:36 UT, the poleward-side brightening arc again broke up in the eastern part of the FOV of the KIAN ASI into two arcs. The poleward-side breakup arc continued to intensify, but does not show bead-like structure clearly. The identifiable brightening spots along the arc were clearly observed in the ISUAL observation (see Sect. 4). Subsequently, at ∼08:29:06 UT a strong arc intensification was observed in the GAKO and WHIT FOVs, and at ∼08:29:27 UT it broke up. Note that the third arc breakup was observed in the FOVs of the GAKO and WHIT ASIs even after the breakup arc expansion started at ∼08:29:12 UT in the FOV of the KIAN ASI. Subsequently, the full substorm expansion unfolded in the FOVs of these three ASIs. The timings of the appearance of the substorm initiation arc and the subsequent three arc breakups are summarized in Table 2.

Table 2. Timings of auroral substorm arc onset and subsequent arc breakups for the 21 December 2006 substorm event.

Time (UT)	Feature of Auroral Substorm
08:27:09	Substorm initiation arc appears at ∼65.5° MLAT
08:27:48	First arc breakup
08:28:36	Second arc breakup
08:29:27	Third arc breakup

For this substorm event, the initial substorm arc appeared at ∼08:27:09 UT and subsequently there were three separate auroral arc breakups at 08:27:48 UT, 08:28:36 UT, and 08:29:27 UT. Before each arc-breakup occurred, there were azimuthally-spaced bright spots along the exponentially brightening arc. As shown in Fig. 3a the distance between the bright spots is ∼115 km (the azimuthal mode number is ∼145) in the KIAN ASI image at ∼08:27:33 UT. Figure 3b shows the evolution of the average arc intensity (in unit of KIAN ASI detector counts) of the initial substorm arc initiated at ∼08:27:04 UT, and the arc first grew with an exponential growth rate of ∼0.021 s^{-1} until 08:27:15 UT and then intensified with a larger growth rate of ∼0.13 s^{-1} until it saturated after 08:27:35 UT (Elphinstone et al., 1995; Voronkov

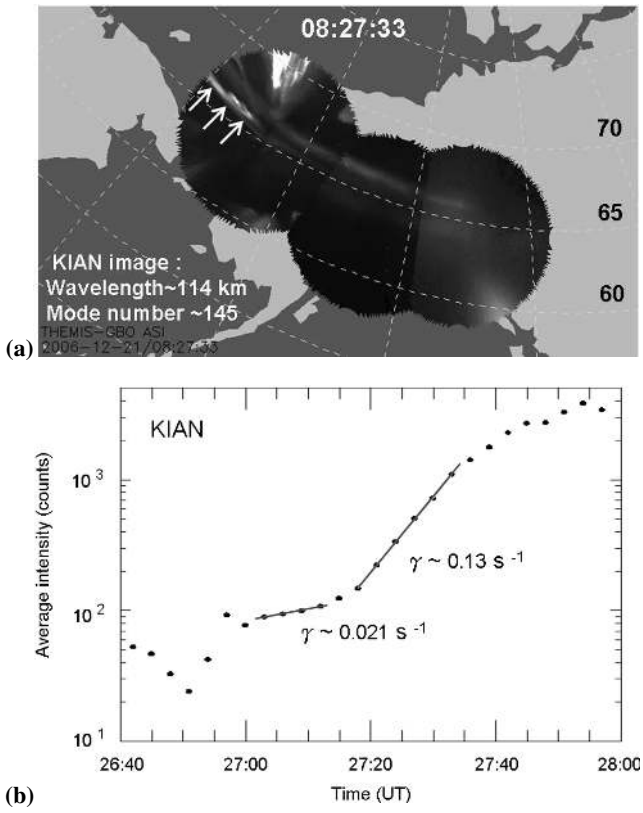

Fig. 3. (a) Auroral substorm initiation arc form appeared in the FOV of the THEMIS ground-based ASI located at KIAN for the 21 December 2006 substorm event, and **(b)** the temporal evolution of the average arc intensity.

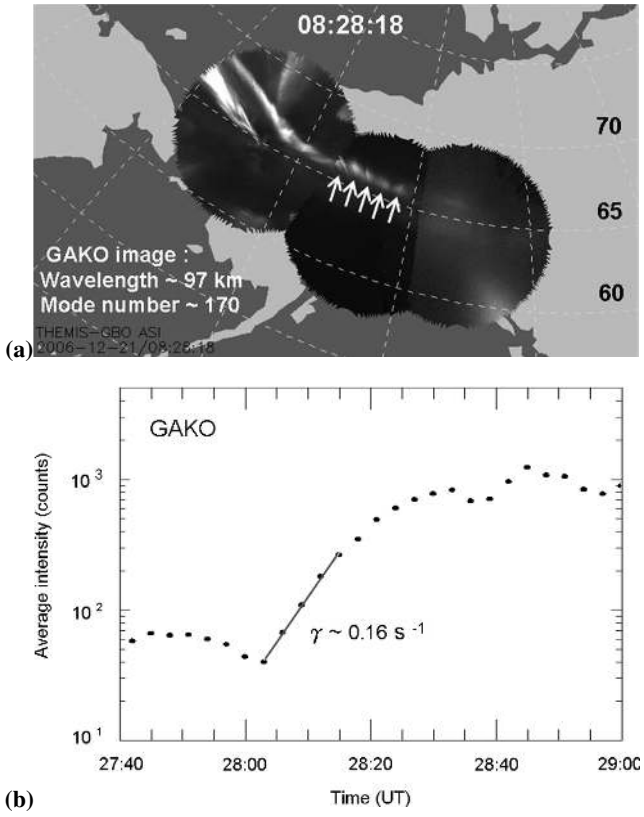

Fig. 4. (a) Auroral arc form observed by the THEMIS ASIs located at KIAN, GAKO, and WHIT for the 21 December 2006 substorm event, and **(b)** the temporal evolution of the average arc intensity.

et al., 2003; Donovan et al., 2008; Liang et al., 2007, 2008; Sakaguchi et al., 2009; Rae et al., 2009a, b, 2010). Note that in determining the breakup arc intensity we have separated the arc intensity from other regions. Before the second arc breakup occurred, the azimuthal mode number of the brightening arc spot structure is ∼170 at 08:28:18 UT as shown in Fig. 4a. During this period the average arc intensity grew exponentially with a growth rate of $\sim 0.16\,s^{-1}$ as shown in Fig. 4b until the second arc broke up at ∼08:28:36 UT. The brightening spots in the third arc was not clearly seen in the ASI images, but was observed clearly by the ISUAL CCD Imager aboard the FORMOSAT-2 satellite which will be described in Sect. 4. These observations suggest that an instability with high azimuthal mode number are responsible for producing the discrete substorm arcs with amplitude growing exponentially until nonlinear effects set in to break up the arcs.

4 Auroral substorm observation by ISUAL/FORMOSAT-2

The 21 December 2006 auroral substorm was also observed by the ISUAL CCD Imager aboard the FORMOSAT-2 satellite in the overlapped FOV region of GAKO and WHIT from 08:28:12–08:30:00 UT. The entire sequence of ISUAL images is given in supplementary material Animation S2. The ISUAL CCD Imager provided clear images of the bright-spot structure during the arc intensification and the third arc breakup at ∼08:29:27 UT as shown in Fig. 5, which shows the representative auroral images in the pre-midnight sector from 08:28:26 UT to 08:29:46 UT observed by the ISUAL CCD Imager at 630 nm filter band, with FWHM of 6 nm (small panels) and their ground projections in the magnetic coordinate (large panels). The arc ground projection was performed by assuming the brightest emission altitude at ∼100 km and the projected ground location is similar to the THEMIS ASI measurement. This is reasonable because >1 keV electrons can deposit most of their energy down to ∼100 km height (Meier et al., 1989; Shiokawa and Fukunishi, 1990) and the N_2(1PG) emissions at 625.3 nm and 632.3 nm (Chamberlain, 1961) can contribute more significantly in the 100–120 km height range in intense aurora arcs

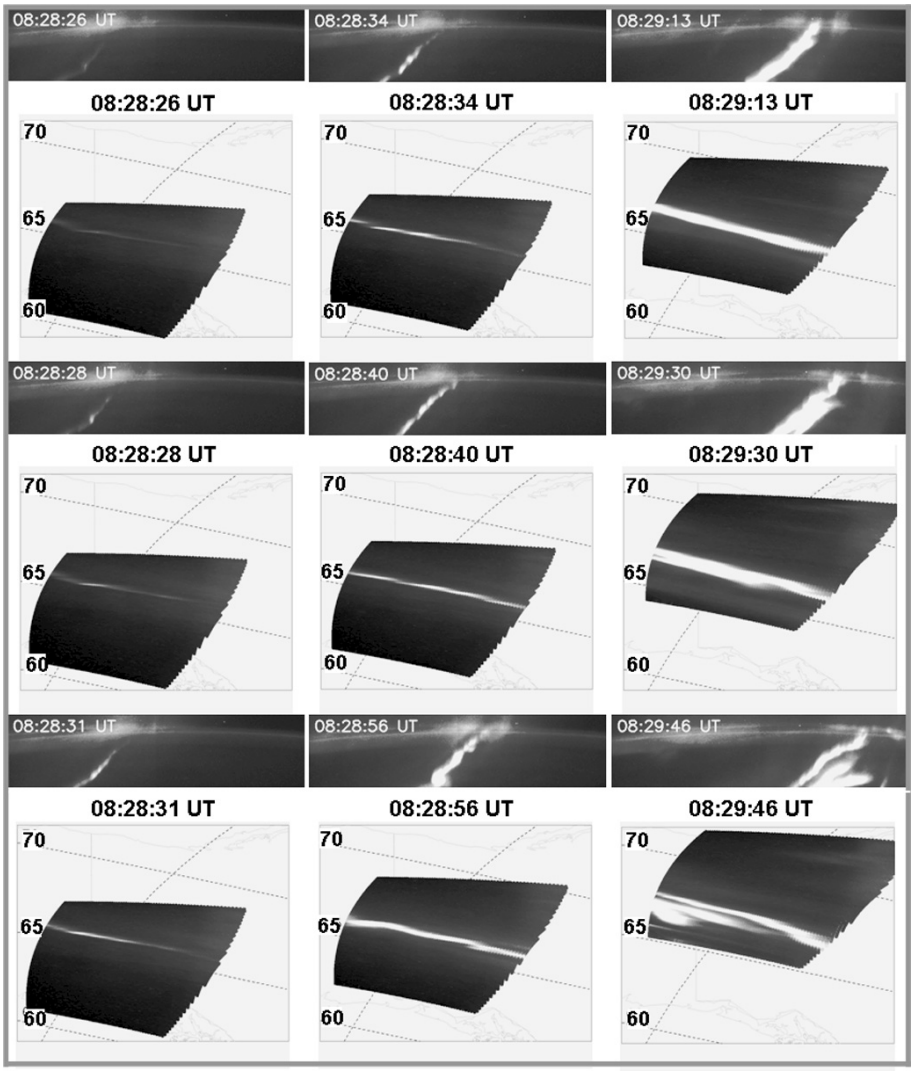

Fig. 5. Auroral arc evolution and breakup of the 21 December 2006 substorm observed by the ISUAL Imager on board the FORMOSAT-2 satellite.

than the 630 nm atomic Oxygen emission that peaks at 200–250 km height.

The FORMOSAT-2 satellite takes 14 revolutions per day in a sun-synchronized orbit at ∼890 km altitude with 99° inclination angle. Its orbit is approximately at 10:30 LT over the dayside equator and 22:30 LT over the night side equator. The ISUAL CCD Imager points eastward of the FORMOSAT-2 satellite orbit when it was in the northward moving direction on the night side. The footprints of the FORMOSAT-2 satellite are shown as squares and the corresponding FOV regions of the ISUAL CCD Imager as trapezoids which are approximately at local pre-midnight from 22:00–23:00 MLT as shown in Fig. 1b. The FOV of the ISUAL CCD Imager is 20° (horizontal) × 5° (vertical) and the image data has 516 × 128 (pixels), which corresponds to a spatial resolution of ∼2 km pixel^{-1} and can reveal the fine structure of substorm breakup arcs. The photon counts are translated into intensity based on the laboratory instrument calibration before the satellite launch (Mende et al., 2005). The ISUAL CCD Imager was operated at a cadence of one image every 1.4 s with 1-s exposure.

From Fig. 5 no active aurora was observed in the ISUAL FOVs in the beginning. But a few seconds later an arc appeared at ∼65.5° MLAT with a width of less than 0.1° in latitude. Subsequently, approximately equally-spaced bright spots appeared along the arc. The bright spots were first identified at ∼08:28:19 UT and continued from 08:28:19 to 08:29:05 UT. The distance between the bright spots was estimated to be ∼96 km (or an azimuthal mode number of ∼173) from the ISUAL arc image at ∼08:28:34 UT as shown in Fig. 6a. After ∼08:29:30 UT the arc intensified and expanded until it broke up into several parts. It is noted that the

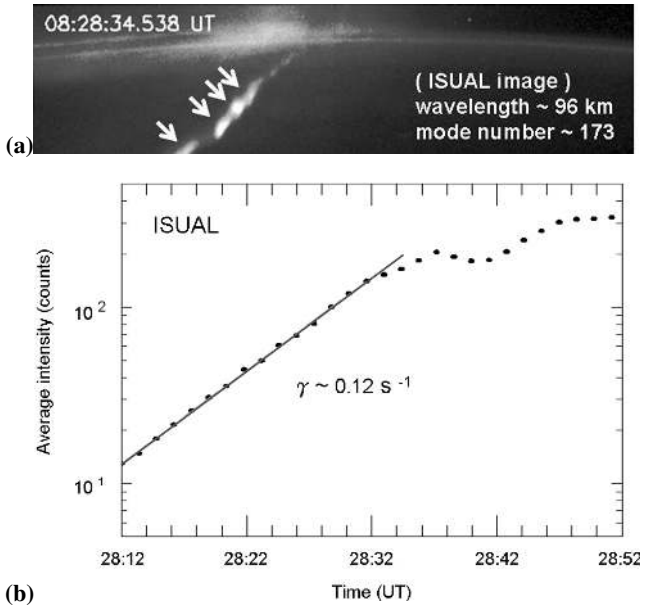

Fig. 6. (a) Auroral arc structure observed by the ISUAL Imager aboard the FORMOSAT-2 satellite, and **(b)** the temporal evolution of the average arc intensity.

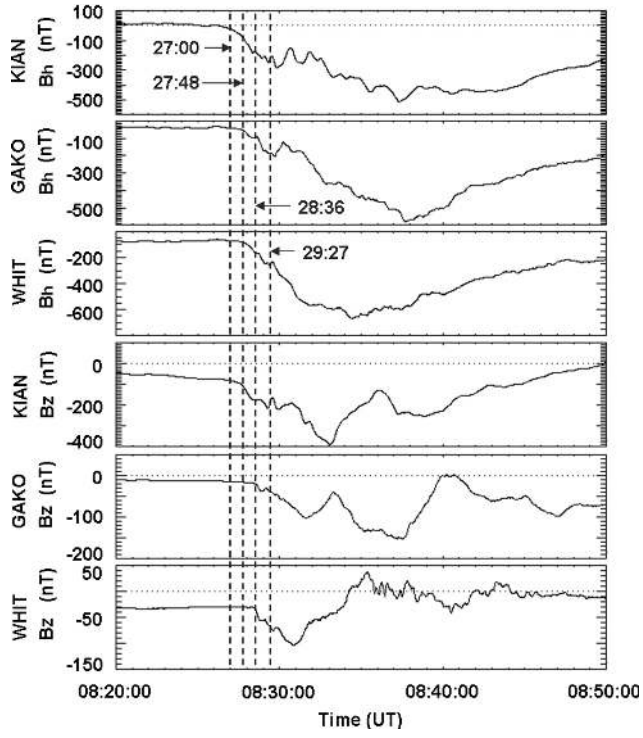

Fig. 7. The H-component and Z-component of 1-s resolution magnetic field (relative to the background dipole field) measured at magnetometer sites from west to east at KIAN, GAKO, and WHIT.

arc evolution and its breakup time approximately coincided with the arc observation by the GAKO and WHIT ASIs as shown in Fig. 2. Figure 6b shows that the average arc luminosity grew exponentially from 08:28:12 UT with the growth rate $\sim 0.12\,s^{-1}$ and then the arc breakup at ~08:29:30 UT. This growth rate is close to the arc intensity growth rate of $\sim 0.16\,s^{-1}$ observed by the GAKO ASI as shown in Fig. 4b.

Note that the observed arc intensity growth rate varies from $\sim 0.13\,s^{-1}$ for the KIAN arc ($m \sim 145$, shown in Fig. 3), $\sim 0.16\,s^{-1}$ for the GAKO arc ($m \sim 170$, shown in Fig. 4), and $\sim 0.12\,s^{-1}$ for the ISUAL arc ($m \sim 173$, shown in Fig. 6). The predicted growth rate of the KBI instability is on the order of O(1/10) of the ion magnetic drift frequency which depends on the azimuthal mode number, and plasma temperature and magnetic field gradient ad curvature in the plasma sheet where the KBI is located. Thus, the predicted KBI growth rate depends on the location of the substorm arc, the most unstable azimuthal mode number and the plasma condition. Therefore, the growth rates for these different arcs are reasonably similar and are consistent with the KBI theory.

5 Auroral substorm arc and westward electrojet

Akasofu et al. (1965) reported that the westward electrojet is rapidly intensified along the brightening arc in the ionosphere. Its magnetic signature on the ground is a sharp decrease (called a negative bay) in the north-south (H) component of the Earth's magnetic field. In order to explain the intense auroral electrojet, Boström (1964) proposed the generation of a Cowling channel by a strong increase of the ionospheric conductivity, which is proportional to the precipitating electron flux. The Cowling channel can be considered as a highly uniform conducting, east–west elongating strip embedded in a larger, but much less conductive region. When a uniform primary westward electric field is imposed on the strip, a primary northward Hall current is driven across the strip. Due to the steep gradient of the conductivity at the north–south edges of the strip, part of this Hall current may flow out to the magnetosphere as a field-aligned current, but the excess Hall current accumulates positive (negative) charges at the northward (southward) boundary of the strip. These charges give rise to a "secondary" southward polarization field, which drives a secondary southward Pedersen current to balance the primary northward Hall current. The secondary electric field also drives a secondary westward Hall current (a strong westward electrojet) in the Cowling channel. The effect of the northward Hall current prevented from flowing, thus resulting in the setup of a polarization electric field, was first investigated by Cowling (1932), and the "Cowling conductivity" was first named by Chapman (1956). The Cowling channel has been studied theoretically and observationally (e.g., Baumjohann and Treumann, 1996; Fujii et al., 2011; Yoshikawa et al., 2011).

In auroral arcs precipitating energetic electrons with energy >1 keV can deposit most of their energy down to ~100–150 km altitude (Meier et al., 1989; Shiokawa and Fukunishi,

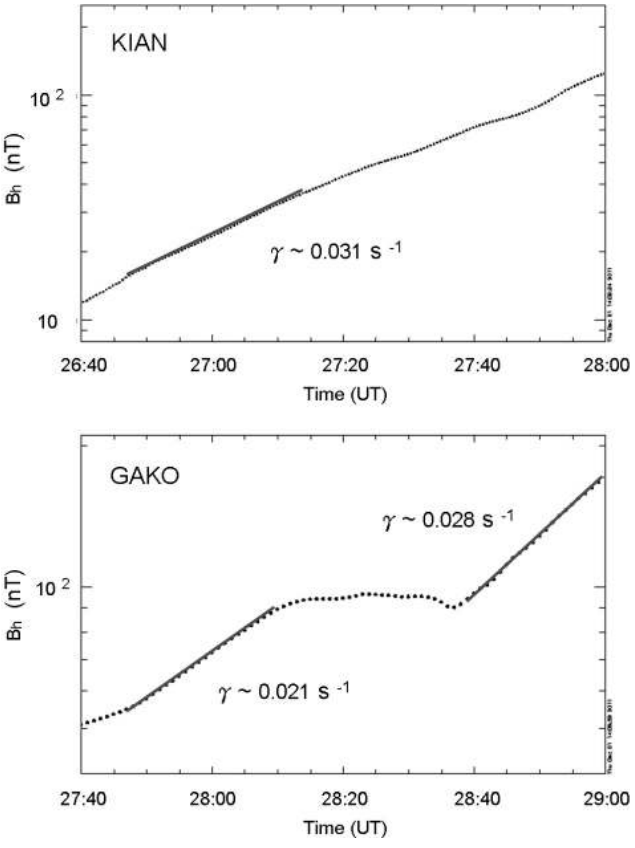

Fig. 8. The growth of the westward electrojet current associated with the arc at KIAN (upper panel) and the arc at GAKO (lower panel), which is proportional to B_h (the decrement of the H-component magnetic field relative to the background dipole field) measured by the ground magnetometer underneath the arc.

1990), thus the westward electrojet can be narrow in both latitude and altitude in the brightening arc. Moreover, the observed arc azimuthal structure indicates that the conductance is non-uniform along the Cowling channel which complicates the electrojet structure. This effect should be considered in future studies.

When a westward electrojet flows in the arc in the northern aurora zone, B_h (the H-component (positive in the northward direction) magnetic field relative to the background dipole field) decreases, and B_z (the Z-component (positive in the upward direction) magnetic field relative to the background dipole field) increases on the poleward side of the arc and decreases on the equatorward side. As shown in Fig. 7, both B_h and B_z at KIAN located at 65.08° MLAT, which is located on the equatorward side of the substorm initiation arc located at ∼65.5° MLAT, started to decrease when the arc was formed at ∼08:27:09 UT, indicating a westward electrojet was formed and intensified together with the substorm initiation arc. After the first arc breakup at ∼08:27:48 UT, the new arc started to move poleward and extend eastward, and B_h, but not B_z, at GAKO and WHIT also started to decrease. However, after the second arc-breakup (at ∼08:28:36 UT) was observed in the eastern part of the KIAN ASI FOV, both B_h and B_z at KIAN, GAKO and WHIT started to decrease rapidly because they were all located on the equatorward side the brightening arc and westward electrojet. After the third arc-breakup (∼08:29:27 UT) occurred in the FOVs of GAKO and WHIT, the auroral substorm started to fully develop, and B_z at GAKO and WHIT decreased further.

Next, we show the temporal correlation between the arc intensity and the westward electrojet current, which is roughly proportional to B_h (the decrement of the H-component magnetic field relative to the background dipole field H-component) measured at the ground magnetometer station underneath the electrojet. Figure 8 shows the evolution of B_h at KIAN (upper panel) and GAKO (lower panel). It is interesting to note that B_h at KIAN increased exponentially with the growth rate of $\sim 0.031\,s^{-1}$ from ∼08:26:40 UT, which is before the substorm initiation arc appeared at ∼08:27:04 UT (shown in Fig. 3b) observed by the KIAN ASI. Similarly, B_h at GAKO increased exponentially with the growth rate of $\sim 0.021\,s^{-1}$ from ∼08:27:50 UT, which is before the exponential growth of the GAKO arc intensity starting at ∼08:28:04 UT (shown in Fig. 4b). However, B_h at GAKO saturated after ∼08:28:10 UT, but again started to increase exponentially with the growth rate of $\sim 0.028\,s^{-1}$ from ∼08:28:40 UT when the second arc breakup was observed at ∼08:28:36 UT.

The results indicate that the exponential growth of the westward electrojet current is correlated with the exponential growth of the arc intensity although at different growth rates. The exponential growth of the westward electrojet current started before the arc was observed by the ASI. The timing difference is probably because the background light noise and sensitivity of the ASI in observing the weak arc emission in the very early phase of arc formation. Thus, it is reasonable to speculate that the westward electrojet is produced concurrently within the auroral arc. This supports the theory of Cowling channel effect on the production of the westward electrojet.

6 Ground Pi1 and Pi2 pulsations and auroral arc intensity

Pi1 and Pi2 fluctuations also exist in the ground-based magnetic field data, and we examine the relative timing of these fluctuations with the substorm arc. Because the H- and Z-components of the ground magnetic field contain the effects of the substorm westward electrojet, we analyze the D-component (in the east–west direction) of the magnetic field perturbation which is least affected by the westward electrojet.

To accurately extract the Pi1 and Pi2 waves, we use an improved Hilbert-Huang Transformation (HHT) method (Huang et al., 1998, 1999, 2003, 2009; Wu and Huang,

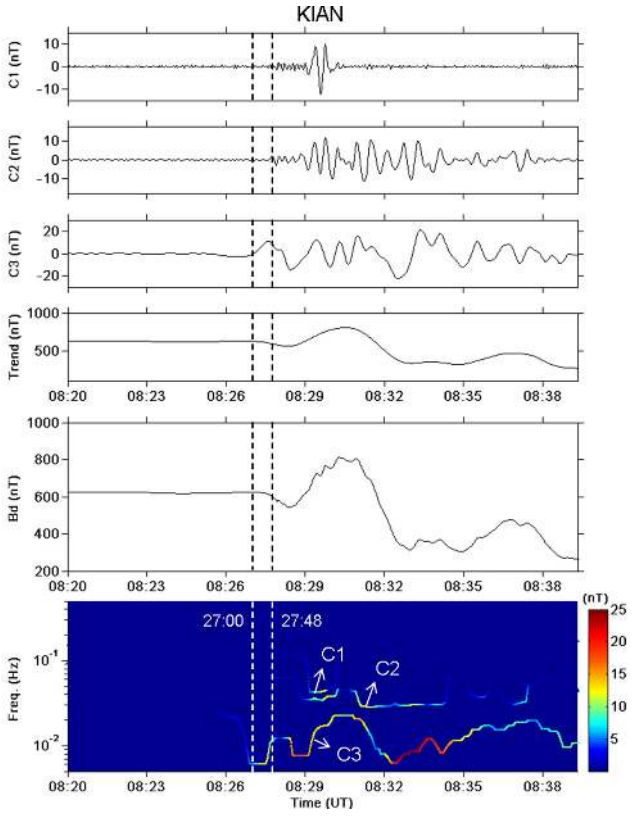

Fig. 9. The HHT analysis of the D-component magnetic field measured at the KIAN magnetometer site. The dashed lines indicate the timings of substorm initiation arc and the first arc breakup.

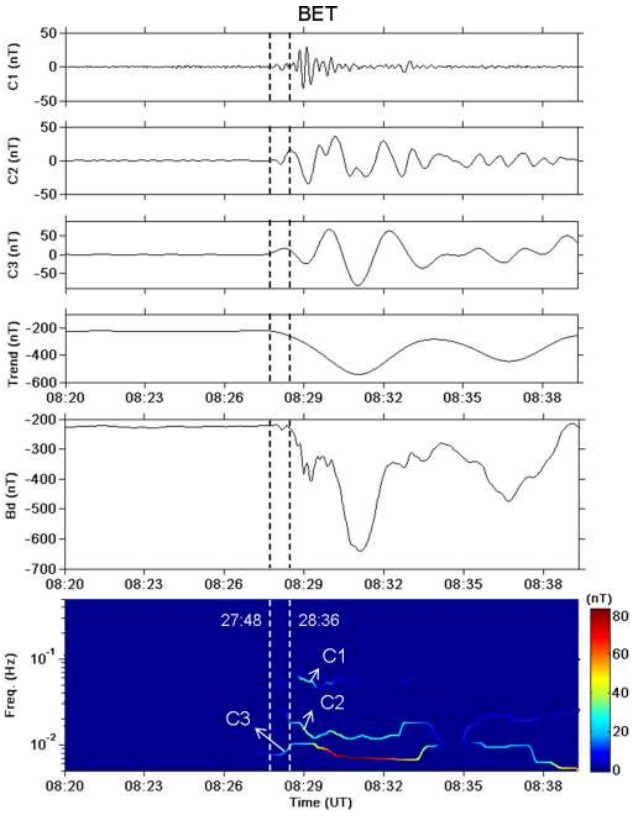

Fig. 10. The HHT analysis of the D-component magnetic field measured at the BET magnetometer site. The dashed lines indicate the timings of the first and second arc breakup.

2004, 2009) to analyze the geomagnetic field data. The HHT method decomposes the nonlinear data into a linear superposition of intrinsic mode functions (IMFs) labeled as C1, C2, C3, etc. Each IMF represents different frequency behavior, where the frequency and amplitude vary with time. Then, the nonlinear "instantaneous frequency" and the "instantaneous amplitude" are computed for each IMF to obtain the amplitude-frequency-time spectrogram, which allows for exploring the physical mechanisms in nonlinear and nonstationary processes. The HHT method has advantages over the Fourier transform and Wavelet transform methods.

Figure 9 shows the D-component magnetic field at the KIAN magnetometer site and its HHT decomposition results. The fifth panel from the top shows the original D-component magnetic field data. The top 2 panels show the HHT decomposition components (C1 and C2) that contain the Pi1 and higher frequency fluctuations. The third panel shows the HHT decomposition component (C3) that contains the Pi2 fluctuations. The fourth panel shows the HHT decomposition trend that represents the background field variation associated with the westward electrojet. The bottom panel shows the amplitude-frequency-time spectrogram of the Pi1 and Pi2 fluctuations (C1, C2, and C3). It is clear that the Pi2 perturbations started to grow almost simultaneously with the appearance of the substorm initiation arc at ∼08:27:09 UT. The higher frequency Pi1 perturbations appeared at the first arc breakup at ∼08:27:48 UT.

After the first arc-breakup in the FOV of the KIAN ASI, the poleward moving breakup arc started to extend eastward to the FOVs of the GAKO and WHIT ASIs at ∼08:28:00 UT. The poleward-side arc was located roughly between the latitudes of the BET and CGO magnetometer sites. Thus, we examine the magnetic fluctuations at these two sites to see whether the breakup arc brightening is related to Pi2 perturbations. Figures 10 and 11 show the D-component magnetic field and its HHT decomposition results (arranged in the same way as in Fig. 9) at the BET and CGO magnetometer sites, respectively. It is clear that at the BET site the Pi2 perturbation started to grow at ∼08:27:48 UT, which roughly coincided with the eastward extension of the poleward-side arc to the GAKO FOV at ∼08:28:00 UT. The Pi1 perturbations started to grow at ∼08:28:36 UT, which is about 50 s later than the appearance of the Pi2 perturbation. Similarly, from Fig. 11 the Pi2 perturbation at the CGO site started to grow at ∼08:28:00 UT and the Pi1 perturbations started to grow at ∼08:28:30 UT, which is about 30 s later than the appearance of the Pi2 perturbation.

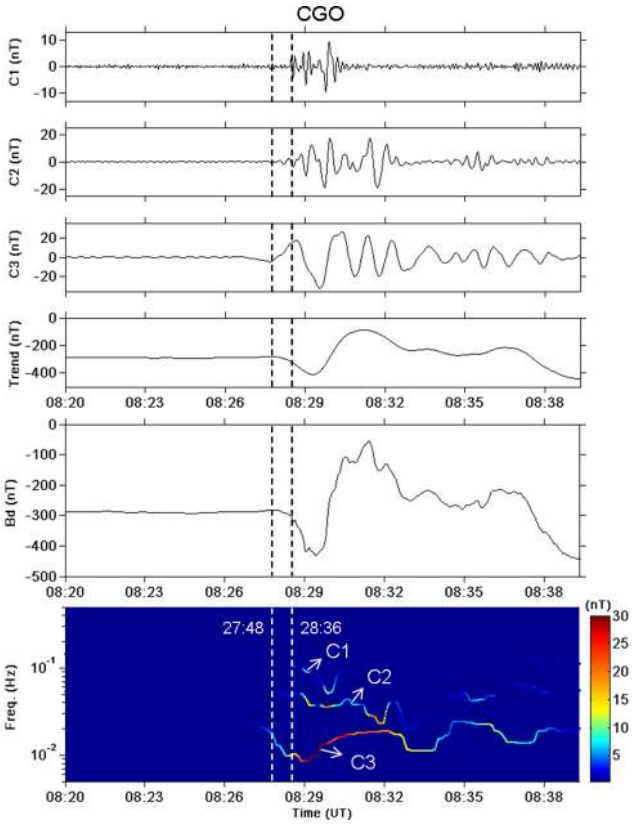

Fig. 11. The HHT analysis of the D-component magnetic field measured at the CGO magnetometer site. The dashed lines indicate the timings of the first and second arc breakup.

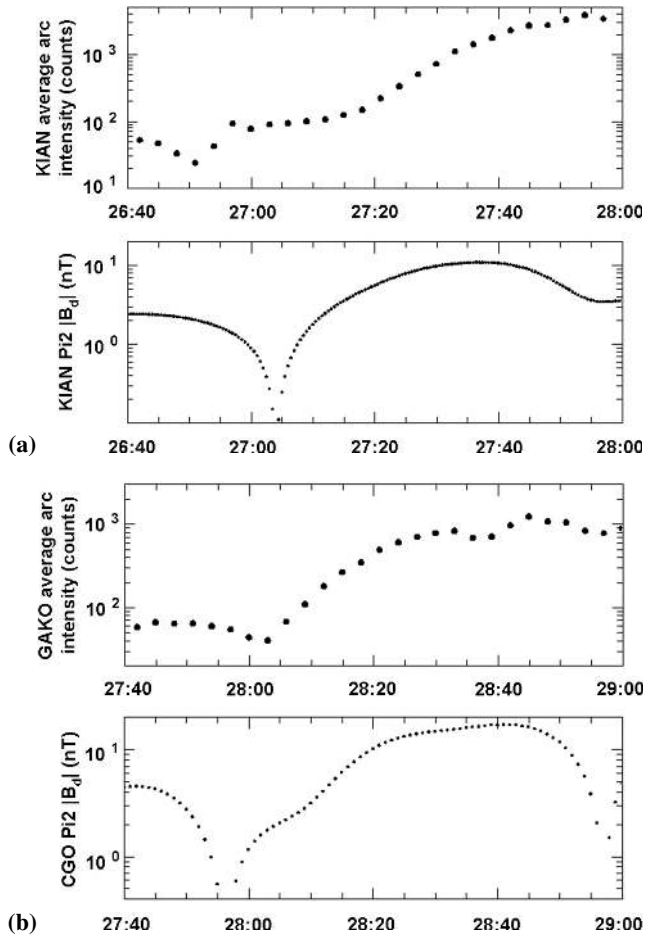

Fig. 12. **(a)** The temporal correlation between the intensity growth of the substorm initiation arcs observed by KIAN ASI and the absolute value of the Pi2 D-component magnetic field observed by the ground KIAN magnetometer which is just underneath the breakup arc. **(b)** The temporal correlation between the intensity growth of the substorm initiation arcs observed by GAKO ASI and the absolute value of the Pi2 D-component magnetic field observed by the ground CGO magnetometer which is just underneath the breakup arc.

From the ground magnetic field data and HHT analysis results shown in Figs. 9–11 we suggest that the Pi2 perturbations are related to the arc formation and intensification. Because the Pi1 perturbations are observed after the Pi2 perturbations grow to larger amplitude, which is about several tens of seconds after the Pi2 perturbations are excited, the Pi1 pulsation is probably not the main cause of substorm arc formation and intensification and breakup. Because Pi2 pulsations are also observed in satellite observations prior to the onset of substorm dipolarization in the plasma sheet and Pi1 waves are also observed at or after the substorm onset (e.g., Takahashi et al., 1987; Roux et al., 1991; Cheng and Lui, 1998; Shiokawa et al., 2005), the Pi1 and Pi2 waves observed in the near-Earth plasma sheet may be the same phenomena as those observed by ground-based magnetometers located under the arc.

Finally, we determine the temporal correlation between the arc intensity and the Pi2 amplitude during the arc intensification phase. Figure 12a shows the temporal evolution of the substorm initiation arc intensity observed by KIAN ASI and the absolute value of the Pi2 D-component magnetic field amplitude at KIAN, which is underneath the substorm initiation arc during the arc intensification phase. It is clear that after the appearance of the substorm initiation arc at ∼08:27:09, the growth and saturation of the arc intensity and Pi2 amplitude are almost concurrent before ∼08:27:50. Figure 12b shows the temporal correlation between the arc intensity observed by GAKO ASI and the absolute value of the Pi2 D-component magnetic field amplitude observed by the ground magnetometer at CGO during the second arc intensification phase, and the consistent growth and saturation behavior between the arc intensity and the Pi2 amplitude is clearly seen. Thus, the temporal correlation between the arc intensity and the Pi2 amplitude further supports the relation between the Pi2 wave and the substorm auroral arc formation.

Table 3. Timings of energetic particle injection observed by geosynchronous satellites for the 21 December 2006 substorm event and the field line footprints of these satellites based on the T-96 model.

Time (UT)	Field line footprints of observing geosynchronous spacecraft	Energetic particle observation
08:28:40	LANL-97A (65.5 MLAT, 19.11 MLT)	First proton flux enhancement
08:29:30	1989-046 (63.5 MLAT, 23.15 MLT)	Electron injections
08:29:45	1994-084 (63.4 MLAT, 22.96 MLT)	Electron injections

7 Energetic particle injection at geosynchronous orbit

To determine whether the substorm region in the plasma sheet is consistent with the auroral activity in the magnetic local time domain, we investigated the energetic particle injection observed by the geosynchronous satellites. The sudden increase of energetic particle flux over a wide range of energy is called the dispersionless energetic particle injection. It is often observed at the geosynchronous orbit and in the radiation belt during magnetospheric substorms (Arnoldy et al., 1969; Baker et al., 1982). During the substorm expansion phase, the magnetic field dipolarization region in the equatorial plane expands both earthward and tailward and particles are swept earthward by the $\boldsymbol{E} \times \boldsymbol{B}$ drift due to the dawn-dusk electric field associated with the magnetic field dipolarization and gain energy via the betatron acceleration process (e.g., Zaharia et al., 2000). While particles are swept earthward by the $\boldsymbol{E} \times \boldsymbol{B}$ drift, protons drift westward and electrons drift eastward via the magnetic gradient and curvature drift motion out of the dipolarization region. Thus, when the dipolarization region expands to the particle drift shell where the observation satellites are located, energetic particles will be observed by the satellites. Because the particle magnetic drift velocity is proportional to the particle kinetic energy, there will be time delay in the observed particle injection depending on the particle energy if the observation point is outside the dipolarization region in longitude. Thus, from the time delay we can estimate how far the observation satellite is away from the expansion front of the dipolarization region in the same particle drift-shell.

In Fig. 13 the top panel shows the energetic proton injection observed by the LANL-97A geosynchronous satellite starting at ~08:28:40 UT, and the middle and bottom panels show the dispersionless energetic electron flux enhancement observed by the 1989-046 geosynchronous satellite starting at ~08:29:30 UT and by the 1994-084 geosynchronous satellite starting at ~08:29:45 UT. If we assume the magnetic field can be approximated by the Tsyganenko's T-96 model, then as shown in Fig. 1 the field line footprint of satellite position was at ~19.11 MLT and 65.5° MLAT for the LANL-97A satellite, and at ~22.96 MLT and 63.4° MLAT for the

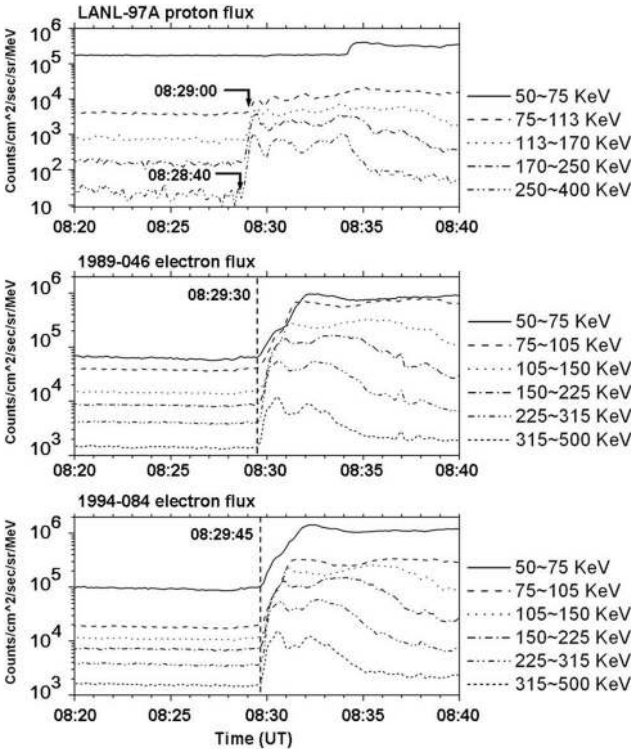

Fig. 13. The energetic particle injection observed by geosynchronous satellites during the 21 December 2006 substorm event.

1994-084 satellite, and at ~23.15 MLT and 63.5° MLAT for the 1989-046 satellite. The timings of energetic particle injections observed by these 3 synchronbous satellites and the field line footprints of these satellites based on the T-96 model are summarized in Table 3.

From the top panel in Fig. 13 the 250–400 keV proton flux enhancement observed by the LANL-97A satellite started at ~08:28:40 UT and the 75–113 keV proton flux enhancement started at ~08:29:00 UT. From the dependence of proton injection timing delay on particle energy, at ~08:28:32 UT the western edge of the dipolarization expansion front is estimated to reach ~6° east in the proton drift-shell longitude to the LANL-97A satellite location if we assume that it took ~8 s for the 400 keV protons with magnetic drift velocity of ~500 km s^{-1} to reach the LANL-97A satellite at ~08:28:40 UT. This magnetic drift velocity is consistent with the estimated value based on the T-96 field. This can approximately account for the timing differences in the observed proton flux enhancement for different energies that it took ~28 s for the 110 keV protons to reach the LANL-97A satellite at ~08:29:00 UT. Although we have no auroral observation west of the FOV of the KIAN ASI, it is reasonable to assume that at the geosynchronous orbit the substorm auroral activity could expand westward to ~6° (or 24 min in MLT) east to the LANL-97A satellite footprint at ~08:28:32 UT to account for the observed energetic proton injection.

On the other hand, the electron injections for all energy channels (50–500 keV) were observed by the 1989-046 satellite at almost the same time at ∼08:29:30 UT, which is the starting time of the full substorm expansion as observed in the FOV of the WHIT ASI. Thus, the 1989-046 satellite was located in the substorm expansion region. However, the electron injections in all energy channels were observed by the 1994-084 satellite almost simultaneously at ∼08:29:45 UT, which indicates that at ∼08:29:45 UT the substorm dipolarization front has expanded earthward and reached near the 1994-084 satellite location, which is located closer to the Earth than the 1989-046 satellite. Thus, the dipolarization region covers a longitudinal range of ∼4 h in MLT at the geosynchronous orbit. The above estimation of the expansion of the dipolarization region to the geosynchronous orbit is consistent with the region of the substorm auroral activity observed by THEMIS ASIs. This also supports that the auroral substorm region maps along field lines to the dipolarization region in the magnetosphere.

8 Summary and discussion

In this study we have presented the main observational features of an auroral substorm event occurred on 21 December 2006. The event is studied by using high temporal and spatial resolution observations by THEMIS GBO (3 s cadence and 1 km resolution at magnetic zenith for All-Sky-Imagers and 2 samples per second for ground magnetometers), the ISUAL CCD Imager aboard the FORMOSAT-2 satellite (1.4 s cadence and 2 km pixel^{-1} resolution), and the geosynchronous satellites. Prior to the auroral substorm, there was a pre-existing arc which remained undisturbed. Then, a faint aurora appeared on the equatorward side of the pre-existing arc at 08:26:36 UT and propagated westward to the edge of KIAN FOV when the substorm initiation arc was observed at ∼08:27:09 UT on the equatorward side latitude of the faint aurora. This faint aurora may be related to the north–south streamers as suggested by Nishimura et al. (2010) and Lyons et al. (2010, 2011) and it may correspond to some flow in the magnetosphere. It is expected that the streamer flows and other magnetospheric plasma transport processes un-identifiable by the ASI auroral observations may bring plasma to the substorm onset region in the near-Earth plasma sheet, and contribute to the build-up of the plasma pressure and its gradient. Then, the kinetic ballooning instability can occur due to the enhanced plasma pressure gradient and magnetic field curvature and drive parallel electric field to accelerate electrons along the field lines into the ionosphere to produce substorm aurora arcs. The azimuthal bead-like structure of the substorm arc should correspond to the azimuthal mode structure of the KBI. The azimuthal arc structure is observable as the parallel electric field amplitude of the KBI grows during the arc intensification.

Before the full auroral substorm expansion onset, three subsequent auroral arc breakups took place with short time separation of ∼1 min, which is much shorter than several minutes reported in typical auroral substorms (e.g., Morioka et al., 2010; Saito et al., 2010). Prior to each arc breakup, azimuthally-spaced brightening spot structures were observed along the arc with arc intensity growing exponentially. The azimuthally-spaced bright spot structure has the azimuthal mode number of ∼100–200. The arc intensity has the growth rate of ∼0.1 s^{-1}. We also analyzed the magnetic field data that are measured by the ground magnetometers located under the arcs, and we found that the Pi2 pulsations appeared almost simultaneously with the arc formation and the Pi2 amplitude grew together with the arc intensification prior to arc breakups. Thus, it is highly possible that the Pi2 perturbations are related to the arc formation. The Pi1 perturbations are excited after the Pi2 pulsations grow to larger amplitude, and co-exist with Pi2 perturbations in the expansion phase (Samson, 1982; Lester, 1984; Cheng and Lui, 1998; Lessard et al., 2007; Morioka et al., 2009, 2010). Thus, Pi1 pulsations are not directly related to the arc formation.

The ballooning mode has been proposed to explain the substorm onset and Pi2 waves observed in the strong cross-tail current region (e.g., Roux et al., 1991; Cheng and Lui, 1998; Lee et al., 1998; Cheng and Zaharia, 2004; Cheng, 2004; Dobias et al., 2004; Saito et al., 2008; Henderson, 2009). The ballooning modes are destabilized by the free energy of plasma pressure gradient that is in the same direction of magnetic field curvature. The increase in the pressure gradient in the near-Earth plasma sheet region due to the enhanced plasma convection (Erickson, 1992) can lead to further thinning of the plasma sheet, and increase of the magnetic field curvature (Zaharia and Cheng, 2003).

Based on the ideal MHD model, the ballooning modes with very large perpendicular wave number (or very high azimuthal mode number ∼O(100)) have been shown to be unstable even for low plasma $\beta(\beta \leq 1)$ in the central plasma sheet for 3-D disturbed time magnetosphere equilibria (Cheng and Zaharia, 2004). However, from satellite observations (e.g., AMPTE/CCE observations) substorms are initiated when the plasma β in the central plasma sheet is well above unity (Lui et al., 1992; Cheng and Lui, 1998; Zaharia and Cheng, 2003; Saito et al., 2008). Moreover, the unstable ideal MHD ballooning mode is purely growing and has no real frequency and no parallel electric field so that electrons can not be accelerated into the ionosphere by the ideal MHD ballooning modes to produce auroral forms. Thus, kinetic effects must be included in the theoretical analysis of ballooning modes.

It has also been demonstrated that by including the kinetic effects of trapped particles, finite ion Larmor radii, wave-particle resonances and finite parallel electric field, the critical plasma β for unstable ballooning modes is greatly enhanced over the ideal MHD theory prediction (Cheng, 1982a, b, 2004; Cheng and Lui, 1998; Cheng and Gorelenkov,

2004). In particular, the kinetic effects of trapped electron dynamics and finite ion gyroradii have large stabilizing effects so that the instability β threshold at equator becomes much larger than unity. However, the wave-particle resonance effect between the kinetic ballooning instability (KBI) and ion magnetic drift allows the release of the pressure gradient free energy and makes the KBI unstable with a plasma β threshold comparable to the observed values in the plasma sheet. Our preliminary KBI calculations showed that the most unstable KBIs are in the strong cross-tail current region that maps to the ionosphere to form an auroral arc form similar to the ideal MHD calculation results (Cheng and Zaharia, 2004). The azimuthal mode number for the most unstable KBIs is on the order of 100–300 due to the ion gyroradius effect. The KBI parallel electric field can accelerate electrons along the field lines into the ionosphere to produce the substorm arcs with azimuthally-spaced bright spot structure. The KBI frequency is on the order of the ion magnetic drift frequency, which is in the Pi2 frequency range in the near-Earth plasma sheet (e.g., Takahashi et al., 1987; Roux et al., 1991; Cheng and Lui, 1998; Shiokawa et al., 2005) and on the ground under the substorm arcs.

Based on the KBI theory for substorm onset, one expects that the KBI amplitude (perturbed electric field and magnetic field) grows exponentially and then saturates by nonlinear effects. Because the Pi2 magnetic perturbations in the near-Earth plasma sheet and on the ground underneath the substorm arcs often show exponential growth before the auroral arc breakup and then saturate afterward, it is reasonable to consider that the Pi2 instabilities observed in the plasma sheet and on the ground are of the same KBI process. Then, we would expect the arc intensity to grow together with the Pi2 amplitude prior to the arc breakup. This is confirmed by the observed temporal growth correlation between the arc intensity and the Pi2 amplitude as shown in Fig. 12.

The observed poleward movement of the poleward side breakup arcs and their subsequent breakup can be explained by the transport process caused by the turbulence produced by the KBI (Pi2 pulsations) and associated Pi1 pulsations in the plasma sheet. When the KBI grows to large amplitude (corresponding to arc intensification), the Pi2 and associated Pi1 pulsations can form an EM turbulence and cause plasma transport which relaxes the local plasma pressure gradient by transporting plasma pressure from the higher pressure side to the lower pressure side (on the tailward side). When some plasma pressure is moved to the tailward side of the pressure profile flattening region, the pressure gradient in the tailward side becomes steeper. As the plasma transport process proceeds, the pressure relaxation region becomes wider, and the tailward side steep pressure gradient region (where the KBI is unstable) moves tailward, which corresponds to the poleward moving breakup arc in the ionosphere. When the pressure gradient in the tailward side region of the plasma pressure flattening region becomes steeper, the KBI can be more intensified and can subsequently cause further breakup of the poleward moving arc in the ionosphere. Similar process can occur in the second poleward moving breakup arc after 082833. Together with observations and analysis results of the high azimuthal mode number bead-like arc structure and the concurrent exponential growth of the arc intensity and the ground Pi2 pulsation amplitude prior to the arc breakup, the KBI theory provides very reasonable interpretation of the occurrences of the brightening arc bead-like structure and arc breakups.

In summary, we have examined the 21 December 2006 substorm event in details. The proposed KBI can reasonably explain many observational features of the 21 December 2006 substorm event. In particular, the Pi2 perturbations are explained as the signature of the KBI, which is excited in the near-Earth plasma sheet and accelerates electrons into the ionosphere to produce arcs. When the KBI grows to large amplitude, it causes plasma transport to relax the plasma pressure profile and thus the current disruption. The higher frequency Pi1 perturbations excited typically after arc breakups are not directly the cause of substorm arc and breakup. However, we caution that instability mechanisms other than the KBI should also be examined for the explanation of the unstable Pi2 pulsation prior to substorm onset (e.g., Lui, 2004), and more careful theoretical and simulational investigations are needed to reach the final conclusion.

Supplementary material related to this article is available online at: http://www.ann-geophys.net/30/911/2012/angeo-30-911-2012-supplement.zip.

Acknowledgements. This work is supported by the National Science Council (Project No. NSC 99-2111-M-006-003) and the Top University Project at the National Cheng Kung University. We thank Harald U. Frey of Space Sciences Laboratory, University of California for providing data from the THEMIS ASIs. We also thank the THEMIS GBO team and GIMA team (Alaska Univ.) for providing the geomagnetic data, the FORMOSAT-2/ISUAL team for providing the ISUAL optical data, Los Alamos National Laboratory for providing the LANL plasma data, and Kyoto World Data Center for Geomagnetism for providing the Dst and AU/AL indices. We also thank Norden E. Huang for discussion on the HHT analysis.

Topical Editor R. Nakamura thanks M. Saito and another anonymous referee for their help in evaluating this paper.

References

Akasofu, S.-I., Kimball, D. S., and Meng, C.-I.: Dynamics of the aurora, II, westward traveling surges, J. Atmos. Terr. Phys., 27, 173–187, 1965.

Akasofu, S.-I., Lui, A. T. Y., and Meng, C.-I.: The importance of auroral features in the search for substorm onset processes, J. Geophys. Res., 115, A08218, doi:10.1029/2009JA014960, 2010.

Angelopoulos, V.: The THEMIS mission, Space Sci. Rev., 141, 5–34, doi:10.1007/s11214-008-9336-1, 2008.

Angelopoulos, V., Baumjohann, W., Kennel, C. F., Coroniti, F. V., Kivelson, M. G., Pellat, R., Walker, R. J., Lühr, H., and Paschmann, G.: Bursty bulk flows in the inner central plasma sheet, J. Geophys. Res., 97, 4027–4039, doi:10.1029/91JA02701, 1992.

Arnoldy, R. L. and Chan, K. W.: Particle substorms observed at the geostationary orbit, J. Geophys. Res., 74, 5019–5028, 1969.

Baker, D. N., Fritz, T. A., and Wilken, B.: Observations and modeling of energetic particles at synchronous orbit on 29 July 1977, J. Geophys. Res., 87, 5917–5932, 1982.

Baker, D. N., Pulkkinen, T. I., Angelopoulos, V., Baumjohann, W., and McPherron, M. L.: Neutral line model of substorms: Past results and present view, J. Geophys. Res., 101, 12975–13010, 1996.

Baumjohann, W. and Treumann, R. A.: Basic space plasma physics, London: Imperial College Press, 1996.

Boström, R.: A model of the auroral electrojets, J. Geophys. Res., 69, 4983–4999, doi:10.1029/JZ069i023p04983, 1964.

Chamberlain, J. W.: Physics of the aurora and airglow, Academic Press, New York, 1961.

Chapman, S.: The electrical conductivity of the ionosphere: A review, Nuovo Cim., 4, Suppl. 4, 1385–1412, doi:10.1007/BF02746310, 1956.

Cheng, C. Z.: High-n collisionless ballooning modes in axisymmetric toroidal plasmas, Nucl. Fusion, 22, 773–785, 1982a.

Cheng, C. Z.: Kinetic Theory of Collisionless Ballooning Modes, Phys. Fluids, 25, 1020–1026, 1982b.

Cheng, C. Z.: Physics of substorm growth phase, onset, and dipolarization, Space Sci. Rev., 113, 207–270, 2004.

Cheng, C. Z. and Gorelenkov, N. N.: Trapped electron stabilization of ballooning modes in low aspect ratio toroidal plasmas, Phys. Plasmas, 11, 4784–4795, 2004.

Cheng, C. Z. and Lui, A. T. Y.: Kinetic ballooning instability for substorm onset and current disruption observed by AMPTE/CCE, Geophys. Res. Lett., 25, 4091–4094, 1998.

Cheng, C. Z. and Zaharia, S.: MHD ballooning instability in the plasma sheet, Geophys. Res. Lett., 31, 6809, doi:10.1029/2003GL018823, 2004.

Chern, J. L., Hsu, R. R., Su, H. T., Mende, S. B., Fukunishi, H., Takahashi, Y., and Lee, L. C.: Global survey of upper atmospheric transient luminous events on the ROCSAT-2 satellite, J. Atmos. Sol. Terr. Phys., 65, 647–659, 2003.

Cowling, T. G.: The electrical conductivity of an ionized gas in the presence of a magnetic field, Mon. Not. R. Astron. Soc., 93, 90–98, 1932.

Dobias, P., Voronkov, I. O., and Samson, J. C.: On linear plasma instabilities during the substorm expansion phase onset, Phys. Plasmas, 11, 2046–2053, doi:10.1063/1.1695357, 2004.

Donovan, E., Liu, W., Liang, J., Spanswick, E., Voronkov, I., Connors, M., Syrjäsuo, M., Baker, G., Jackel, B., Trondsen, T., Greffen, M., Angelopoulos, V., Russell, C. T., Mende, S. B., Frey, H. U., Keiling, A., Carlson, C. W., McFadden, J. P., Glassmeier, K. H., Auster, U., Hayashi, K., Sakaguchi, K., Shiokawa, K., Wild, J. A., and Rae, I. J.: Simultaneous THEMIS in situ and auroral observations of a small substorm, Geophys. Res. Lett., 35, L17S18, doi:10.1029/2008GL033794, 2008.

Elphinstone, R. D., Hearn, D. J., Cogger, L. L., Murphree, J. S., Singer, H., Sergeev, V., Mursula, K., Klumpar, D. M., Reeves, G. D., Johnson, M., Ohtani, S., Potemra, T. A., Sandahl, I., Nielsen, E., Persson, M., Opgenoorth, H., Newell, P. T., and Feldstein, Y. I.: Observations in the vicinity of substorm onset: Implications for the substorm process, J. Geophys. Res., 100, 7937–7969, 1995.

Erickson, G. M.: A quasi-static magnetospheric convection model in two-dimensions, J. Geophys. Res., 97, 6505–6522, 1992.

Fujii, R., Amm, O., Yoshikawa, A., Ieda, A., and Vanhamäki, H.: Reformulation and energy flow of the Cowling channel, J. Geophys. Res., 116, A02305, doi:10.1029/2010JA015989, 2011.

Henderson, M. G.: Observational evidence for an inside-out substorm onset scenario, Ann. Geophys., 27, 2129–2140, doi:10.5194/angeo-27-2129-2009, 2009.

Huang, N. E., Shen, Z., Long, S. R., Wu, M. C., Shih, E. H., Zheng, Q., Tung, C. C., and Liu, H. H.: The empirical mode decomposition method and the Hilbert spectrum for non-stationary time series analysis, Proc. Roy. Soc. Lond., 454A, 903–995, 1998.

Huang, N. E., Shen, Z., and Long, R. S.: A new view of nonlinear water waves – the Hilbsert spectrum, Ann. Rev. Fluid Mech., 31, 417–457, 1999.

Huang, N. E., Wu, M. L., Long, S. R., Shen, S. S., Qu, W. D., Gloersen, P., and Fan, K. L.: A confidence limit for the empirical mode decomposition and the Hilbert spectral analysis, Proc. Roy. Soc. Lond., 459A, 2317–2345, 2003.

Huang, N. E., Wu, Z., Long, S. R., Arnold, K. C., Chen, X., and Blank, K.: On instantaneous frequency, Adv. Adap. Data Anal., 1, 177–229, 2009.

Kepko, L. and McPherron, R. L.: Comment on "Evaluation of low-latitude Pi2 pulsations as indicators of substorm onset using Polar ultraviolet imagery" by K. Liou et al., J. Geophys. Res., 106, 18919–18922, 2001.

Lee, L. C., Zhang, L., Otto, A., Choe, G. S., and Cai, H. J.: Entropy antidiffusion instability and formation of a thin current sheet during geomagnetic substorms, J. Geophys. Res., 103, 29419–29428, 1998.

Lessard, M. R., Lotko, W., LaBelle, J., Peria, W., Carlson, C. W., Creutzberg, F., and Wallis, D. D.: Ground and satellite observations of the evolution of growth phase auroral arcs, J. Geophys. Res., 112, A09304, doi:10.1029/2006JA011794, 2007.

Lester, M., Hughes, W. J., and Singer, H. J.: Longitudinal structure in Pi 2 pulsations and the substorm current wedge, J. Geophys. Res., 89, 5489–5494, 1984.

Liang, J., Liu, W. W., Spanswick, E., and Donovan, E. F.: Azimuthal structures of substorm electron injection and their signatures in riometer observations, J. Geophys. Res., 112, A09209, doi:10.1029/2007JA012354, 2007.

Liang, J., Donovan, E. F., Liu, W. W., Jackel, B., Syrjäsuo, M., Mende, S. B., Frey, H. U., Angelopoulos, V., and Connors, M.: Intensification of preexisting auroral arc at substorm expansion phase onset: Wave-like disruption during the first tens of seconds, Geophys. Res. Lett., 35, L17S19, doi:10.1029/2008GL033666, 2008.

Liou, K., Meng, C.-I., Lui, A. T. Y., Newell, P. T., Brittnacher, M., Parks, G., Reeves, G. D., Anderson, R. R., and Yumoto, K.: On relative timing in substorm onset signature, J. Geophys. Res., 104, 22807–22817, 1999.

Liou, K., Meng, C.-I., Newell, P. T., Takahashi, K., Ohtani, S.-I., Lui, A. T. Y., Brittnacher, M., and Parks, G.: Evaluation of low-latitude Pi2 pulsations as indicators of substorm onset using Polar ultraviolet imagery, J. Geophys. Res., 105, 2495–2505, 2000.

Lui, A. T. Y.: Current disruption in the Earth's magnetosphere: Observations and models, J. Geophys. Res., 101, 13067–13088, 1996.

Lui, A. T. Y.: Potential plasma instabilities for substorm expansion onsets, Space Sci.. Rev., 113, 127–206, 2004.

Lui, A. T. Y., Chang, C. L., Mankofsky, A., Wong, H. K., and Winske, D.: A cross-field current instability for substorm expansion, J. Geophys. Res., 96, 11389–11401, 1991.

Lui, A. T. Y., Lopez, R. E., Anderson, B. J., Takahashi, K., Zanetti, L. J., McEntire, R. W., Potemra, T. A., Klumpar, D. M., Greene, E. M., and Strangeway, R.: Current disruptions in the near-Earth neutral sheet region, J. Geophys. Res., 97, 1461–1480, doi:10.1029/91JA02401, 1992.

Lyons, L. R., Voronkov, I. O., Donovan, E. F., and Zesta, E.: Relation of substorm breakup arc to other growth-phase auroral arcs, J. Geophys. Res., 107, 1390, doi:10.1029/2002JA009317, 2002.

Lyons, L. R., Nishimura, Y., Xing, X., Angelopoulos, V., Zou, S., Larson, D., McFadden, J., Runov, A., Mende, S., and Fornacon, K. H.: Enhanced transport across entire length of plasma sheet boundary field lines leading to substorm onset, J. Geophys. Res., 115, A00I07, doi:10.1029/2010JA015831, 2010.

Lyons, L. R., Nishimura, Y., Kim, H.-J., Donovan, E., Angelopoulos, V., Sofko, G., Nicolls, M., Heinselman, C., Ruohoniemi, J. M., and Nishitani, N.: Possible connection of polar cap flows to pre- and post-substorm onset PBIs and streamers, J. Geophys. Res., 116, A12225, doi:10.1029/2011JA016850, 2011.

Meier, R. R., Strickland, D. J., Hecht, J. H., and Christensen, A. B.: Deducing composition and incident electron spectra from ground-based auroral optical measurements: A study of auroral red line processes, J. Geophys. Res., 94, 13541–13552, 1989.

Mende, S. B., Frey, H. U., Hsu, R. R., Su, H. T., Chen, A. B., Lee, L. C., Sentman, D. D., Takahashi, Y., and Fukunishi, H.: D region ionization by lightninginduced electromagnetic pulses, J. Geophys. Res., 110, A11312, doi:10.1029/2005JA011064, 2005.

Mende, S. B., Angelopoulos, V., Frey, H. U., Harris, S. E., Donovan, E., Jackel, B., Syrjaesuo, M., Russell, C. T., and Mann, I.: Determination of substorm onset timing and location using the THEMIS ground based observatories, Geophys. Res. Lett., 34, L17108, doi:10.1029/2007GL030850, 2007.

Mende, S. B., Harris, S. E., Frey, H. U., Angelopoulos, V., Russell, C. T., Donovan, E., Jackel, B., Greffen, M., and Peticolas, L. M.: The THEMIS array of ground based observatories for the study of auroral substorms, Space Sci. Rev., 141, 357, doi:10.1007/s11214-008-9380-x, 2008.

Meng, C.-I. and Liou, K.: Substorm timings and time scales: A new aspect, Space Sci. Rev., 113, 41–75, 2004.

Morioka, A., Miyoshi, Y., Tsuchiya, F., Misawa, H., Yumoto, K., Parks, G. K., Anderson, R. R., Menietti, J. D., and Honary, F.: Vertical evolution of auroral acceleration at substorm onset, Ann. Geophys., 27, 525–535, doi:10.5194/angeo-27-525-2009, 2009.

Morioka, A., Miyoshi, Y., Miyashita, Y., Kasaba, Y., Misawa, H., Tsuchiya, F., Kataoka, R., Kadoura, A., Mukai, T., Yumoto, K., Menietti, D. J., Parks, G., Liou, K., Honary, F., and Donovan, E.: Two-step evolution of auroral acceleration at substorm onset, J. Geophys. Res., 115, A11213, doi:10.1029/2010JA015361, 2010.

Nishimura, Y., Lyons, L., Zou, S., Angelopoulos, V., and Mende, S.: Substorm triggering by new plasma intrusion: THEMIS allsky imager observations, J. Geophys. Res., 115, A07222, doi:10.1029/2009JA015166, 2010.

Rae, I. J., Mann, I. R., Angelopoulos, V., Murphy, K. R., Milling, D. K., Kale, A., Frey, H. U., Rostoker, G., Russell, C. T., Watt, C. E. J., Engebretson, M. J., Moldwin, M. B., Mende, S. B., Singer, H. J., and Donovan, E. F.: NearEarth initiation of a terrestrial substorm, J. Geophys. Res., 114, A07220, doi:10.1029/2008JA013771, 2009a.

Rae, I. J., Mann, I. R., Murphy, K. R., Milling, D. K., Parent, A., Angelopoulos, V., Frey, H. U., Kale, A., Watt, C. E. J., Mende, S. B., and Russell, C. T.: Timing and localization of ionospheric signatures associated with substorm expansion phase onset, J. Geophys. Res., 114, A00C09, doi:10.1029/2008JA013559, 2009b.

Rae, I. J., Watt, C. E. J., Mann, I. R., Murphy, K. R., Samson, J. C., Kabin, K., and Angelopoulos, V: Optical characterization of the growth and spatial structure of a substorm onset arc, J. Geophys. Res., 115, A10222, doi:10.1029/2010JA015376, 2010.

Roux, A., Perraut, S., Robert, P., Morane, A., Pedersen, A., Korth, A., Kremser, G., Aparicio, B., Rodgers, D., and Pellinen, R.: Plasma sheet instability related to the westward traveling surge, J. Geophys. Res., 96, 17697–17714, doi:10.1029/91JA01106, 1991.

Saito, M. H., Miyashita, Y., Fujimoto, M., Shinohara, I., Saito, Y., Liou, K., and Mukai, T.: Ballooning mode waves prior to substorm-associated dipolarizations: Geotail observations, Geophys. Res. Lett., 35, L07103, doi:10.1029/2008GL033269, 2008.

Saito, M. H., Miyashita, Y., Fujimoto, M., Liou, K., Saito, Y., and Sigwarth, J. B.: Stepwise feature of aurora during substorm expansion compared with the nearEarth tail dipolarizations: Possible types of substorm dynamics, J. Geophys. Res., 115, A02207, doi:10.1029/2009JA014572, 2010.

Sakaguchi, K., Shiokawa, K., and Donovan, E.: Azimuthal structures of ray auroras at the beginning of the auroral substorm, Geophys. Res. Lett., 36, L23106, doi:10.1029/2009GL041252, 2009.

Samson, J. C.: Pi 2 pulsations: High latitude results, Planet. Space Sci., 30, 1239–1247, 1982.

Samson, J. C., Wallis, D. D., Hughes, T. J., Creutzberg, F., Ruohoniemi, J. M., and Greenwald, R. A.: Substorm intensifications and field line resonances in the nightside magnetosphere, J. Geophys. Res., 97, 8495–8518, 1992.

Shiokawa, K. and Fukunishi, H.: Depedences of auroral 5577 A and 6300 A emission rate on thermospheric density variations, Proc. NIPR Symp. Upper Atmos. Phys., 3, 24–31, 1990.

Shiokawa, K., Baumjohann, W., Haerendel, G., Paschmann, G., Fennell, J. F., Friis-Christensen, E., Lühr, H., Reeves, G. D., Russell, C. T., Sutcliffe, P. R., and Takahashi, K.: High speed ion flow, substorm current wedge, and multiple Pi2 pulsations, J. Geophys. Res., 103, 4491–4507, 1998.

Shiokawa, K., Shinohara, I., Mukai, T., Hayakawa, H., and Cheng, C. Z.: Magnetic field fluctuations during substorm-associated dipolarizations in the nightside plasma sheet around $X = -10\,R_E$, J. Geophys. Res., 110, A05212, doi:10.1029/2004JA010378, 2005.

Takahashi, K., Zanetti, L. J., Lopez, R. E., McEntire, R. W., Potemra, T. A., and Yumoto, K.: Disruption of the magnetotail current sheet observed by AMPTE/CCE, Geophys. Res. Lett.,

14, 1019–1022, 1987.

Uritsky, V. M., Liang, J., Donovan, E., Spanswick, E., Knudsen, D., Liu, W., Bonnell, J., and Glassmeier, K. H.: Longitudinally propagating arc wave in the pre-onset optical aurora, Geophys. Res. Lett., 36, L21103, doi:10.1029/2009GL040777, 2009.

Voronkov, I., Friedrich, E., and Samson, J. C.: Dynamics of the substorm growth phase as observed using CANOPUS and SuperDARN instruments, J. Geophys. Res., 104, 28491–28505, 1999.

Voronkov, I. O., Donovan, E. F., and Samson, J. C.: Observations of the phases of substorms, J. Geophys. Res., 108, 1013, doi:10.1029/2002JA009314, 2003.

Wien, R. G. and Gordon, G.: Characteristics of the development of the westward electrojet during the expansive phase of magnetospheric substorms, J. Geophys. Res., 80, 2109–2128, 1975.

Wu, Z. and Huang, N. E.: A study of the characteristics of white noise using the empirical mode decomposition method, Proc. Roy. Soc. Lond., A, 460, 1597–1611, 2004.

Wu, Z. and Huang, N. E.: Ensemble empirical mode decomposition: A noise-assisted data analysis method, Adv. Adap. Data Anal., 1, 1–41, 2009.

Yoshikawa, A., Nakamizo, A., Amm, O., Vanhamäki, H., Fujii, R., Tanaka, Y.-M., Uozumi, T., Yumoto, K., and Ohtani, S.: Selfconsistent formulation for the evolution of ionospheric conductances at the ionospheric E region within the MI coupling scheme, J. Geophys. Res., 116, A09223, doi:10.1029/2011JA016449, 2011.

Zaharia, S. and Cheng, C. Z.: Near-Earth thin current sheets and Birkeland currents during substorm growth phase, Geophys. Res. Lett., 30, 1883–1886, 2003.

Zaharia, S., Cheng, C. Z., and Johnson, J. R.: Particle transport and energization associated with disturbed magnetospheric Events, J. Geophys. Res., 105, 18741–18752, 2000.